ELSEVIER

Nuclear Instruments and Methods in Physics Research A 419 (1998) 217–229

NUCLEAR INSTRUMENTS & METHODS IN PHYSICS RESEARCH Section A

High-resolution electro-magnetic calorimetry with noble liquids

D. Schinzel[1]

CERN, CH-1211 Geneva 23, Switzerland

Abstract

Electromagnetic calorimeters with noble liquids and their limits in resolution are discussed. The origins of "initial" current measurement in calorimetry are retraced and the performance and first results of the NA48 calorimeter (quasi-homogeneous calorimeter with longitudinal electrode structure) are presented. Results of the prototype calorimeters of KEDR (quasi-homogeneous calorimeter with transverse electrode structure) and of ATLAS (sampling calorimeter with longitudinal electrode structure), are summarized.

1. Introduction

The energy resolution of an electromagnetic calorimeter is usually written as the square root over the quadratic sum of three terms

$$\frac{\sigma(E)}{E} = \frac{a}{E} \oplus \frac{b}{\sqrt{E}} \oplus c. \quad (1)$$

The noise term a takes into account the electronic noise, pile-up and the radioactivity of the active and/or inactive medium. The term b is the square root of the quadratic sum of four terms, which are the sampling fluctuations, the fluctuations due to lateral escape, the Landau fluctuation and the intrinsic shower fluctuations due to the signal generating process. In noble liquid electromagnetic calorimeters, the contribution of the latter two are negligible. Landau fluctuation play an important role only in low-density shower counters. Intrinsic fluctuations are negligible, since the W values of liquid argon and liquid krypton are typically seven orders of magnitude smaller when compared to interesting incident energies above 1 GeV. The quantity W is defined as the energy expended per ion pair. As a matter of fact, losses of roughly a factor of 50 can be tolerated in the signal-generating process without interfering with the "stochastic" term b of the energy resolution. This article will outline a possible reduction of sampling fluctuation in exchange for tolerable losses in signal. The constant term c takes into account intercalibration errors between cells, inhomogeneities and energy absorbing material in front of the calorimeter. In a certain sense, c can be considered as the quality factor of a calorimeter. Constructional and mechanical errors will reflect themselves in a larger constant term. The stochastic term b and the constant term are often used to make comparisons between calorimeters without taking into account that calorimeters are built for specific experiments. These

[1] Member of the NA-48 Collaboration.

0168-9002/98/$19.00
PII: S0168-9002(98)00795-5

may require excellent time and space resolution in exchange for a slightly worsened energy resolution.

Calorimetry with noble liquids, like liquid argon or liquid krypton exhibit a certain number of advantages: their response is uniform, various electrode geometries are possible, they allow direct calibration, since the signal generating process is proportional to the incident energy. In addition, they are fast if limited to the measurement of the initial current. However, they may be difficult to build, not only because of associated cryogenics.

2. Electromagnetic showers

The resolution of an electromagnetic calorimeter is limited by fluctuations of the elementary processes through which the energy of an incoming particle is degraded. In addition, realistic electromagnetic calorimeters have finite dimensions leading to further deterioration in resolution.

Longitudinal and transverse shower development have been discussed in many excellent review articles [1–7]. This article will briefly retrace classical shower theory in a pictorial way. It covers mainly quasi-homogeneous calorimeters and fast sampling calorimeters, both of which measure the initial current.

High-energy electrons and photons interact with matter mainly through bremsstrahlung and pair production, respectively. Through these interactions, secondary photons and electron–positron pairs are produced which in turn interact in the same fashion, thus producing a cascade of charged and non-charged particles. The growth of the cascade will stop when the energies of the secondaries fall below the domain, where radiation losses are dominant. The remaining secondaries will dissipate their energy through ionization. The energy at which radiation losses balance collision losses is called "critical" energy and denoted by ε. For the description of an electromagnetic cascade, three quantities are sufficient, the radiation length X_0, describing the longitudinal shower development, the critical energy ε defined as above and the attenuation length λ_{att}, which describes the slow, exponential decay of the shower after the shower maximum. The lateral spread of the shower is described by the Molière radius R_{M}, which is related to the radiation length X_0 and the ratio of the scattering energy and the critical energy ε. It is mainly due to multiple scattering of non-radiating electrons with large enough energies to travel far from the shower axis. Fig. 1 shows the development of a "classical" shower in the first few radiation lengths. The incoming electron loses in the first radiation length X_0 all but $1/e$ of its energy E through bremsstrahlung. The photon generated by bremsstrahlung will produce an electron–positron pair within its mean free path, which is $\frac{9}{7}X_0$. This pair will continue interacting in the same way as the incoming electron, and so forth. After the second radiation length, the energy of the incoming electron has been degraded to E/e^2. After n radiation lengths the growth of the shower will stop, since the energy has been degraded to $E/e^n = \varepsilon$, the critical energy. The cascade has reached its maximum after $n = \ln(E/\varepsilon)$ generations. Since n indicates the number of cascade generations in units of the radiation length X_0, it is evident, that the shower maximum moves logarithmically with incident energy. The longitudinal shower profiles of a 10 and a 100 GeV shower are shown together in Fig. 2. The shower maximum has moved by a factor of ln(10).

After the shower maximum, the electromagnetic cascade decays exponentially, as $\exp^{(-t/\lambda_{\mathrm{att}})}$, consisting mainly of electrons below critical energy and low-energy photons. The quantity t denotes the longitudinal shower axis in units of X_0. The attenuation length λ_{att} is practically independent of energy, and its value is close to the material-

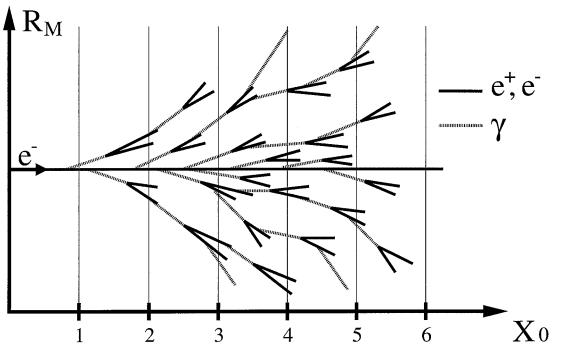

Fig. 1. Development of a "classical" shower.

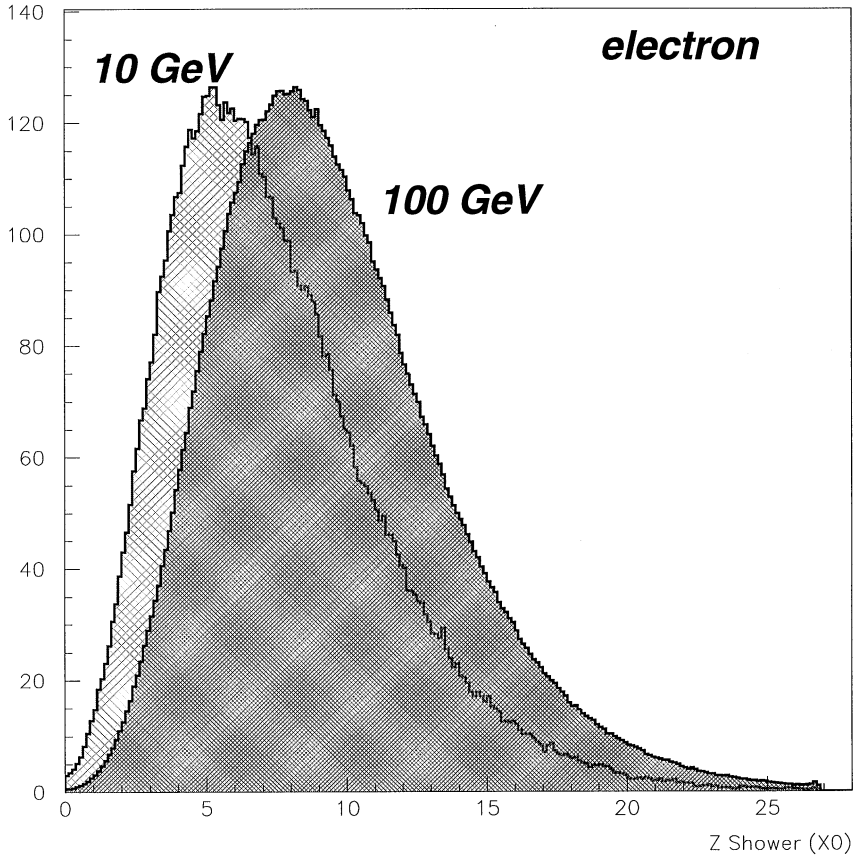

Fig. 2. Longitudinal shower profile, calculated by GEANT for electrons of 10 and 100 GeV entering the NA48 liquid krypton calorimeter.

dependent minimum attenuation for photons. The photons in the tail of the shower dissipate their energy mainly through Compton scattering and photo-effect.

Fig. 3a and b show, respectively, the photons and the charged particle tracks from an electro-magnetic cascade created by an electron of 100 GeV entering into liquid krypton. The cascade has been calculated using GEANT. The zigzag lines, of which the significance will be explained below, are spaced by 1 cm. The cascade is plotted using as units the radiation length X_0 and the Molière radius R_M, respectively. One recognizes clearly the growth of the shower starting after one radiation length. The shower maximum is reached after $\sim 9X_0$. Furthermore 95% of the shower is contained in a radius which equals $2R_M$, indicated by the two straight lines running parallel to the radiation length axis. Lateral position resolution of a fine grain calorimeter is therefore directly related to the Molière radius. In general, the grain is often chosen to be $\sim \frac{1}{2}R_M$. An electro-magnetic shower counter records only the tracks of charged shower particles. Along these tracks the noble liquid is ionized. The sum of all track elements is proportional to the energy of the incident electron. The summed track length T looks indeed as though the electron behaves as a "minimum ionizing" particle that loses an amount of energy equal to the critical energy ε whilst traveling a distance which is equal to the radiation length X_0.

$$T = \sum_{i=1}^{N} T_i = \frac{E}{\varepsilon/X_0}. \tag{2}$$

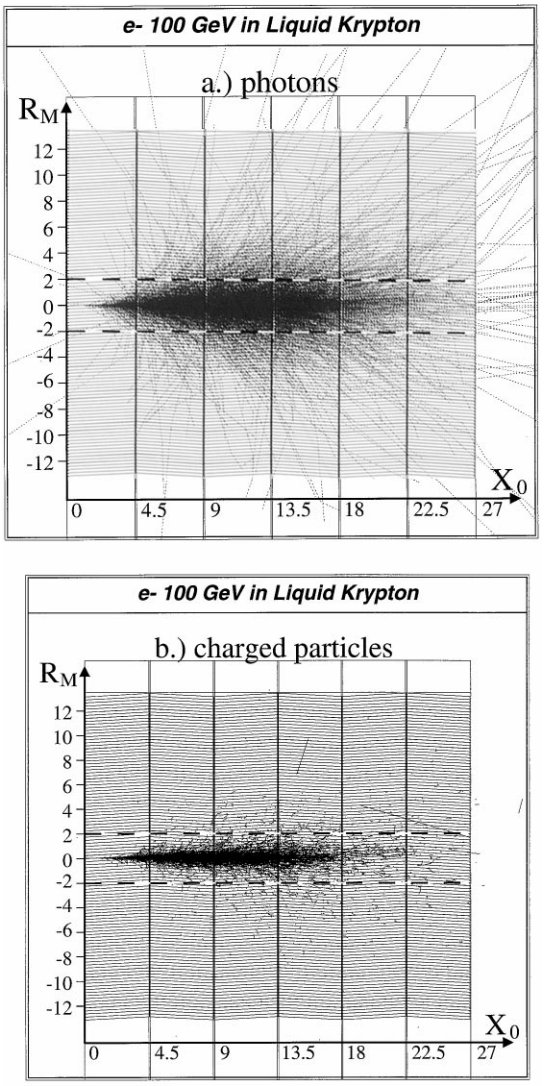

Fig. 3. Electromagnetic cascade of a 100 GeV electron entering the NA48 liquid krypton calorimeter (GEANT). Photons (a), charged shower particles (b).

The upper summation index N gives the number of track elements, over which the summation runs. From shower to shower, the number of track elements N fluctuate. This fluctuation determines the intrinsic energy resolution. In order to get an estimate on the size of N, the length of an elementary track element has to be known. A possible approach is outlined: one assumes that the shortest conceivable track length, the elementary track element, is the distance between two adjacent ionization clusters. The number N is obtained by dividing the track length T by the length of the elementary track element. A rough estimate is obtained in the following way: The diameter of an ionization cluster is of the order of 1–2 nm. The mean energy loss of a minimum ionizing charged shower particle is typically 100 eV per collision, resulting in the creation of 4–5 ion pairs. From the minimum energy loss of a charged shower particle, ne calculates the number of ionization clusters per cm N_C or directly the inverse of this number yielding the length L of an elementary track element. Each elementary track element fluctuates in length. However, the fluctuation of T will be reduced, since the energy of the incident particle is fixed, or in other words, it does not fluctuate [8]. This reduction is taken into account by the Fano factor. Hence, the intrinsic resolution of a homogeneous electromagnetic calorimeter can be written in the following way:

$$\frac{\sigma(E)}{E}=\frac{\sigma(T)}{T}=\frac{\sqrt{F}}{\sqrt{N}}=\frac{\sqrt{F}\cdot\sqrt{L\cdot\varepsilon/X_0}}{\sqrt{E}}\cong\frac{\sqrt{F}\sqrt{W}}{\sqrt{E}}. \tag{3}$$

The finite resolution of such an ideal calorimeter is given by the fluctuations in track length. A few numbers for liquid krypton, calculated from above are: the number of clusters $N_c = 22600/\text{cm}$, corresponding to a cluster distance of 450 nm, indicating clearly that adjacent clusters are independent from each other. The intrinsic resolution for 1 GeV incident energy is roughly 0.01%. However, the approach leading to this result is purely academic. Any calorimeter, close to the ideal one, would be dominated by Landau fluctuations, which can normally be neglected in noble liquid calorimetry. Indeed, the detector, which is closest to the ideal one, is ICARUS [9,10], a homogeneous 600 ton liquid argon detector. Its resolution, as far as the stochastic term is concerned, should mainly be limited by Landau fluctuations.

In a realistic calorimeter, shower energies down to 0 eV cannot be measured. The minimum energy of a charged shower particle that can be detected is called E_c, the cut-off energy. The higher the cut-off energy E_c, the shorter will be the track

length. The fractional useful track length is given by

$$T(z) = F(z)\frac{E}{\varepsilon}X_0 \tag{4}$$

where $z = 2.3E_c/\varepsilon$ and $F(z) = e^z\{1 + z\ln(z/1.526)\}$. The function $F(z)$ can be calculated using "Approximation B" by Rossi [11]. In this approximation, first all shower particles undergo a constant energy loss ε/X_0 and second the cross-sections for pair production and bremsstrahlung at all energies are described by the asymptotic formulae for large energies. One of the consequences of this approximation is that, cum grano salis, all results are identical and material independent.

Homogeneous "ideal" electromagnetic calorimeters without realistic electrodes have been considered up to this point. Real calorimeters consist of active and passive material, dividing the incident energy into visible and non-visible energy. If the ratio $E_{vis}/E = 1$, the shower counter is called "homogeneous". For the case that E_{vis}/E is close to one, the calorimeter is called "quasi-homogeneous". If $E_{vis}/E \ll 1$, the shower detector is called "sampling" calorimeter. The active material is the noble liquid, the passive material consists of parallel electrodes spaced at equal distances d from each other, forming ionization chambers. The distance d is called "sampling" thickness. In analogy to the concept of track elements leading to the resolution of an ideal homogeneous detector, one now records the number N of track elements per distance d:

$$N = \frac{T(z)}{d} = F(z)\frac{EX_0}{\varepsilon\ d}. \tag{5}$$

Since there is no correlation between adjacent gaps for reasonable absorber thicknesses, the error of N is the statistical error, namely $\sqrt{N}$. Therefore, one obtains for the resolution

$$\frac{\sigma(E)}{E} = \frac{\sigma(T)}{T} = \frac{1}{\sqrt{N}} = \sqrt{\varepsilon d/F(z)E\cdot X_0}. \tag{6}$$

The resolution of the calorimeter is, as for the homogeneous calorimeter, determined by the fluctuation in track length. Since the shower energy, deposited in a realistic calorimeter, is split into visible and non-visible energy, the track length itself is divided into two parts, one proportional to the visible energy, the other proportional to the non-visible energy. "Sampling" fluctuations describe therefore the fluctuations in energy sharing between active and passive layers. The "non-visible" track length fluctuation dominate the resolution of a sampling calorimeter, since the bulk part of the energy is dissipated in the higher density of the absorber plates. Due to energy conservation, there is off course a strong correlation between visible and non-visible energy and their respective fluctuations.

Space and rate limitations in an experiment very often require, that the electrodes are made of high-density material in order to obtain smaller longitudinal and lateral calorimeter dimensions, respectively. The electrodes can be arranged to form a single gap chamber or interleaving two absorber plates with a thin read-out electrode, to form a double gap chamber. The electrodes may be orientated at any angle with respect to the incident beam. They can be perpendicular to the incident beam, as in the liquid argon calorimeters MARS [12] and MARS-2 [13] or the liquid krypton calorimeter KEDR [14], or they can have strong longitudinal zigzag structures like the "accordion"-shaped ATLAS liquid argon calorimeter [15] or longitudinal structures zigzagging slightly as in case of the NA48 liquid krypton calorimeter [16].

The first liquid argon sampling calorimeter was built by Willis and Radeka [17] in 1974. The calorimeter used 1.5 mm thick iron plates as absorber, spaced by 2 mm liquid argon as sensitive medium. Only 20% of the incident energy is seen by the liquid argon gap. The stochastic term of the energy resolution was found to be $7.4\%/\sqrt{E}$, where E is given in GeV. Applying formula 6, one obtains $\sigma(E)/E = 8.6\%/\sqrt{E}$, assuming a cut-off energy of 0.5 MeV. The energy E inserted under the square root of Eq. (6) is not anymore the incident energy but it is the visible energy E_{vis}, since the number of track elements per gap is equivalent to the visible energy. Eq. (6) for the energy resolution of a "sampling" calorimeter can therefore be

rewritten in the following way:

$$\frac{\sigma(E)}{E} = \frac{1}{\sqrt{N_{\text{vis}}}} = \sqrt{\varepsilon d/F(z)\kappa E X_0} \tag{7}$$

where $\kappa = E_{\text{vis}}/E$.

3. Initial current measurement

In order to obtain better energy resolution, Eq. (7), used so far to calculate the resolution of an electromagnetic calorimeter with an approximate accuracy of 15% or better, suggests to decrease the ratio d/X_0 more and more. Indeed, the stochastic term b decreases, however, the noise term a increases quadratically, since the detector capacitance increases. Another possibility to improve the energy resolution of a shower counter is to increase the factor $\kappa = E_{\text{vis}}/E$ in Eq. (7), which determines the number of track elements per distance d. This means to get closer to "homogeneous" calorimetry without ever reaching it. Large liquid gaps and thin absorber plates seem to be the solution to the problem. This indeed reduces the sampling fluctuations, which are due to the energy sharing between active and passive layers of the calorimeter. However, it also increases (sampling) fluctuations, which are due to non-uniform signal collection efficiency in the active layer [13,17,18].

In an ionization chamber gap of an electromagnetic shower counter, secondary shower particles can either uniformly ionize the gap by traversing it fully or they can partially ionize the gap by being absorbed or created anywhere in the gap. The current due to the ion pairs produced by ionizing shower particles, assumes either a triangular shape in the case of uniform ionization or a square shape with attached triangle in the case of non-uniform ionization [13,17,18]. Fig. 4 shows both types of ionization together with their corresponding currents, which are the origin of the longitudinal position dependence. Cerri et al. [13] investigated possible solutions to minimize the fluctuations due to longitudinal position dependence. Both solutions are based on signal clipping, which corresponds to the measurement of the initial current in the wide liquid argon gap of a quasi-homogeneous

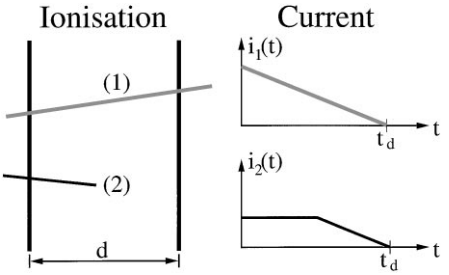

Fig. 4. Uniform and non-uniform ionization and their corresponding currents.

electromagnetic calorimeter. The signal can either be clipped directly at the source by adding a sufficient amount of electro-negative impurities (scavengers) into the liquid argon resulting in an effective charge attenuation or it can be clipped electronically by integrating the signal for short time compared to the total drift time. Both ways result in the measurement of the initial fraction of the current in the gap.

The currents in the liquid argon gap of the electromagnetic shower counter in presence of scavengers can be written in the following way:

$$i_{\text{un}}(t) = N_{\text{e}} \frac{v_{\text{d}}}{d} \left(1 - \frac{t}{t_{\text{d}}}\right) \text{e}^{-t/\tau}, \tag{8}$$

$$i_{\text{nu}}(t) = N_{\text{e}} \frac{v_{\text{d}}}{d} \, \text{e}^{-t/\tau}, \tag{9}$$

where Eqs. (8) and (9) describe uniform and non-uniform ionization of the liquid argon gap, respectively. The quantity τ is the electron lifetime, i.e. the time during which the electron is free and during which it can induce its charge on the read-out electrode. N_{e} is the number of ion pairs produced in a gap of width d. The quantity v_{d} is the drift velocity of the electrons. Rewriting Eqs. (8) and (9) in a single equation yields:

$$i_{\text{un}}(t) = i_{\text{nu}}(t) - N_{\text{e}} \frac{v_{\text{d}}}{d} \cdot \frac{t}{t_{\text{d}}} \text{e}^{-t/\tau} \approx i_{\text{nu}}(t). \tag{10}$$

For small electron lifetimes, say $\tau = \frac{1}{20} t_{\text{d}}$ as it is the case for the MARS-2 calorimeter [13], the uniform and the non-uniform current are practically the same, as can be seen from Eq. (10). The quantity t_{d} denotes the time, which the electron needs to

cross the gap. The resulting reduction in sampling fluctuation is due to the fact that the detector "sees" only the first part of the current, or in other words, the "initial" current. As a consequence, a strong reduction in signal is observed. However, it can be shown that the signal/noise ratio of a wide gap shower detector with "initial" current read-out, as described above, is the same as the one made in a traditional way, namely out of many thin gaps in between thin absorber plates [13].

Reformulating the expression d/X_0 using the velocity of the drifting electrons v_d, one obtains $d/X_0 = t_d/T_{X_o}$, where T_{X_o} denotes the drift time, which is necessary to cover one radiation length. Insertion of t_d/T_{X_o} into Eq. (7) yields the following relation:

$$\frac{\sigma(E)}{E} = \frac{1}{\sqrt{N_{vis}}} = \sqrt{\varepsilon t_d / F(z)\kappa E T_{X_o}}. \quad (11)$$

The quantity t_d is originally the time, which an electron needs to cross the gap of an ionization chamber. However, it will from now on denote the signal clipping time, i.e. the time during which the electron induces its charge on the read-out electrode. This time can either be the integration time of an electronics circuit (shaping time) or it can be the electron lifetime. Both cases are equivalent. Their meaning is that a number n of "fictitious" electrodes is entered into to the wide gap of a shower counter. These fictitious electrodes are spaced by a distance, which is covered by a drifting electron in the time τ, or they are spaced by a distance, corresponding to the shaping time t_i.

Two shower detectors [12,13], one sampling calorimeter with charge integrating read-out consisting of many narrow active gaps and thin passive absorber plates and one quasi-homogeneous calorimeter with initial current read-out made of wide active gaps and few thin electrodes, were tested. Their results are compared with each other in Table 1. Both calorimeters give the same results, as far as sampling fluctuations are concerned, indicating that the above made arguments are correct. The resolution due to sampling fluctuations of a "Gedanken"-calorimeter built like MARS-2, but with charge integrating read-out, would be $\sim 10.6\%/\sqrt{E}$ in the worst case, as calculated from Eq. (7). If ever built, the resolution of such a calorimeter would probably be better, due to "natural" clipping, i.e. short electron lifetime.

Table 1
Comparison of results from two calorimeters.

	MARS	MARS-2
Read out	Charge Q	Current I
Drifttime	1.1 μs	16 μs
Integration time	1.1 μs	0.8 μs
Active layer	1.9 mm	28 mm
Structure	6288 signal strips	315 signal strips
	x strips	x, u, v strips
	Pitch 62.5 mm	Pitch 101 mm
	394 HV planes	45 ground planes
Sampling fluctuation		
Measured $\sigma(E)/E$	$3.6\%\sqrt{E}$	$4\%\sqrt{E}$
Calculated with Eqs. (7) and (11), resp.	$3.9\%\sqrt{E}$	$4.04\%\sqrt{E}$

The best resolution, so far published in noble liquid calorimetry, is the one obtained in the prototype of the quasi-homogeneous KEDR [14] calorimeter. Their sampling fluctuation term is $1.6\%/\sqrt{E}$.

4. Current-sensitive calorimeters with longitudinal read-out

In all of the previously discussed electromagnetic calorimeters, the ionization chambers of the shower counters were orientated perpendicular to the incident particles. The signal collecting electrodes were equipped with striplines, which allows an off-line formation of longitudinal towers. The disadvantage of these structures are, that ambiguities may arise at higher rates, i.e. energy reconstruction may only be possible in one of the views. In addition, integration or clipping times in the order of 1 μs did not make these calorimeters very suited for high-rate environments, as for instance for high-luminosity fixed target or high-luminosity collider experiments. In order to make noble liquid calorimetry suited for future high-rate experiments like the CP violation experiment NA48 at CERN or the ATLAS experiment at the future Large Hadron Collider, new concepts had to be injected into

this field. These concepts were mainly developed in the RD3 collaboration [19], where longitudinal electrode structures and unprecedented short shaping times were introduced. Starting from these new ideas, rapid progress in noble liquid calorimetry was achieved mainly in NA48 and ATLAS.

Electrodes, which are arranged in beam direction, are easily grouped in towers. For sampling calorimetry, like in ATLAS, two longitudinal absorber electrodes, made of stainless steel cladded lead, are interleaved by one 3-layer kapton read-out electrode. Incident particles might impinge on the absorber plates, dissipating their energy mainly therein. This occurrence is avoided by giving the above described cell structure an "accordion" geometry. The geometry of the ATLAS Barrel electromagnetic calorimeter is shown in Fig. 5. The detector depth is ~ 50 cm, corresponding to $26X_0$. The thickness of the lead absorber plates ranges from 0.12 cm, for pseudorapidities larger than 0.8, to 0.18 cm close to the center of the detector. The liquid argon double gap is 2×2 mm. The signal shaping time is 40 ns. Further relevant details of the ATLAS liquid argon calorimetry can be found in the technical design report [20] and in the performance report [21]. Since Fournier [15] presented prototype results of NA48 and ATLAS at this conference three years ago, only the most important results of the prototype of the ATLAS electromagnetic barrel calorimeter are summarized. The energy resolution of the ATLAS prototype barrel calorimeter [15] is shown in Fig. 6. The sampling term agrees well with the result obtained from Eq. (11). The response uniformity [21] is shown in Fig. 7, demonstrating the quality of this prototype. The measured time resolution is $(1.2/E \oplus 0.25)$ ns, which is largely sufficient for bunch crossing identification at the Large Hadron Collider. The noble liquid calorimetry of ATLAS is presently under construction. More test are planned for autumn 1998.

The 24 ton quasi-homogeneous liquid krypton calorimeter [22] was installed into the CP violation

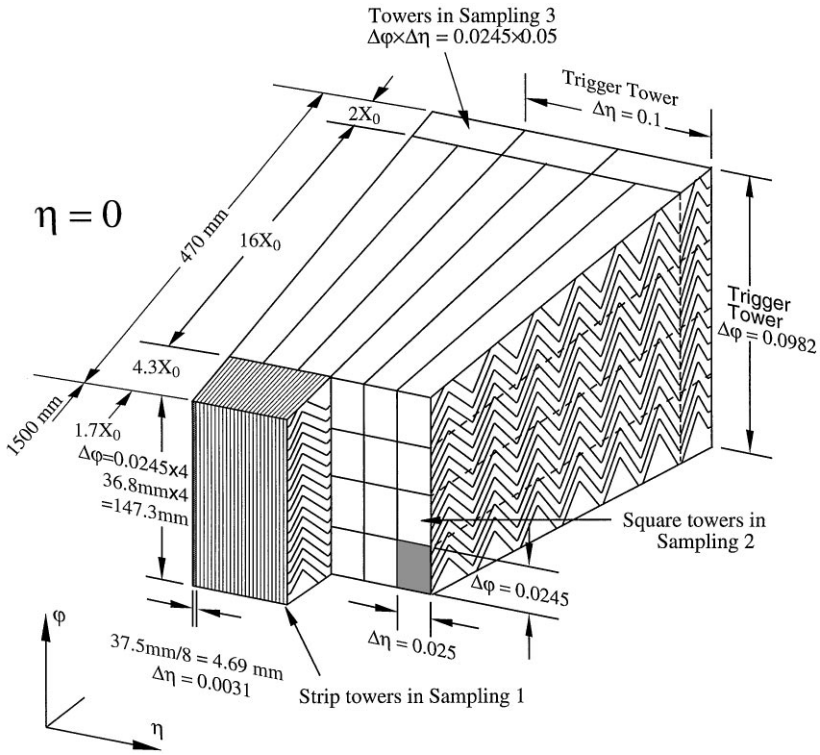

Fig. 5. Read-out granularity of the ATLAS electromagnetic calorimeter.

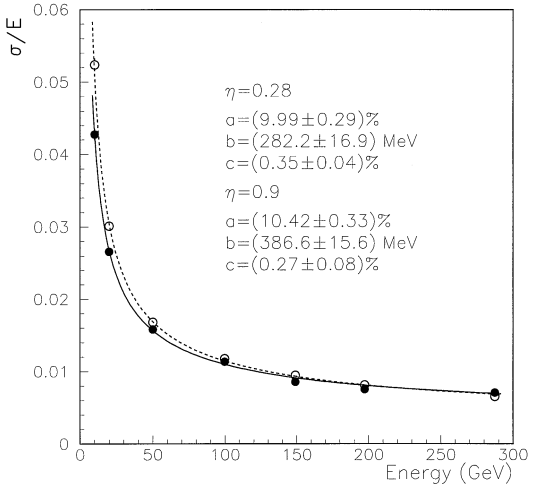

Fig. 6. Energy resolution measured with the ATLAS Barrel prototype calorimeter.

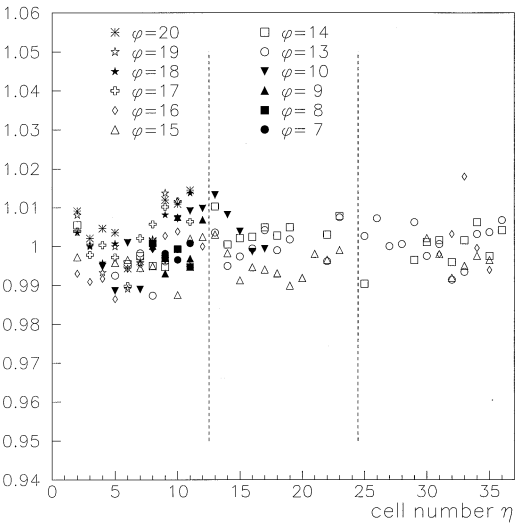

Fig. 7. Cell-to-cell uniformity of the ATLAS liquid argon Barrel prototype.

experiment NA48 at CERN in summer 1996. The electrodes, oriented parallel to the incident particles are made of 40 μm thick CuBe sheets. One cell consisting of three CuBe ribbons spaced by 1 cm forms a 2 cm × 2 cm tower. One cell has a length of $26X_0$ and a width of $\sim \frac{1}{2}R_M$. Since the response of the cell depends on the distance between the impinging particle and the center read-out electrode, the CuBe ribbons are guided by 5 spacer plates to

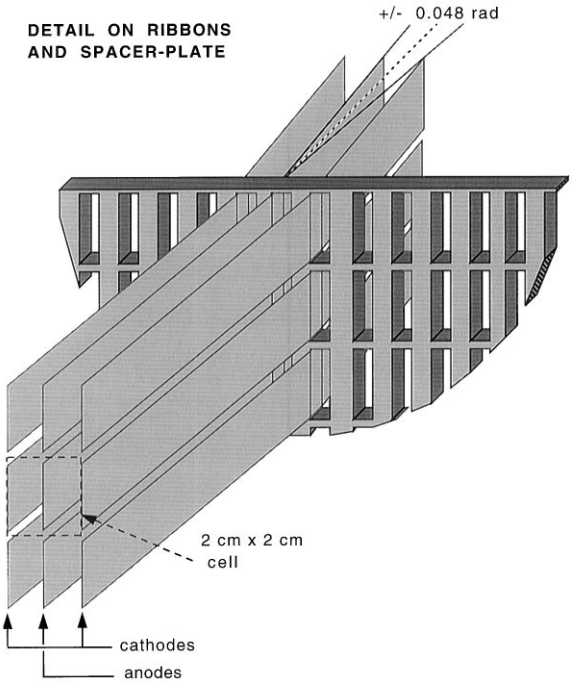

Fig. 8. Read-out cells with CuBe electrodes and spacer plate.

perform a slight longitudinal zigzag. The impact point dependence is therefore reduced and can be represented by a unique correction function, which is the same for all cells [16]. Fig. 8 shows the details of the read-out cell together with one spacer plate and the slight zigzag angle of 100 mrad. The active surface of the detector extends from a radius of 8 cm to an octagon shaped outer boundary. The circle, which can be drawn inside the octagon has a radius of 128 cm. The ribbons are stretched between two base plates. Spacer plates and base plates are made of Stesalit, an epoxy-fiberglass composite material. The total number of CuBe ribbons mounted inside these boundaries is 26 632, forming 13 248 cells. Since the structure is longitudinal, the expressions cell and tower have the same meaning. To satisfy experimental requirements, the transverse dimensions of the cells increase slightly, by 1.1%, between the front plate and the back plate forming a projective geometry. The cell to cell dimensional errors are less than 50 μm. Each cell is read out by an amplifier housed after the back plate inside the liquid krypton vessel. The calorimeter is

housed inside a stainless-steel vessel, which is contained in the outer aluminium vacuum vessel. The thickness of the entrance windows is equal to 4 mm of Al and 3.1 mm of stainless steel. The total material in front of the active volume of the calorimeter corresponds to $\sim 0.6X_0$.

The electronics for read-out and calibration of this detector is described in great detail elsewhere [23–26]. However, for the sake of completeness, a very short description is given here. The front-end electronics is directly mounted on the back-plate of the detector. The preamplifiers are connected to the cells with the shortest possible lead, to optimize speed of signal extraction. The calibration system is located in immediate vicinity to the preamplifiers. Signals similar to the ones of a uniformly ionizing particle are injected into the input of the preamplifiers. The output signals of the preamplifiers are sent via coaxial cables to the feedthroughs, which are located at the top of the cryostat. The transceivers are mounted directly on the feedthroughs. They restore and amplify the original current signal of the cell. Differential drivers send the signal from the transceivers to the digitizers, where the signals are shaped with 75 ns and digitized using 40 MHz FADCs.

The NA48 liquid krypton calorimeter was first tested in a short dedicated test run in the experimental area of NA48. First data taking runs measuring direct CP violation were started in summer 1997. Preliminary results of special runs giving the performance of this detector is discussed in Ref. [27]. Fig. 9 shows the cell-to-cell response of the liquid krypton calorimeter, which is uniformly

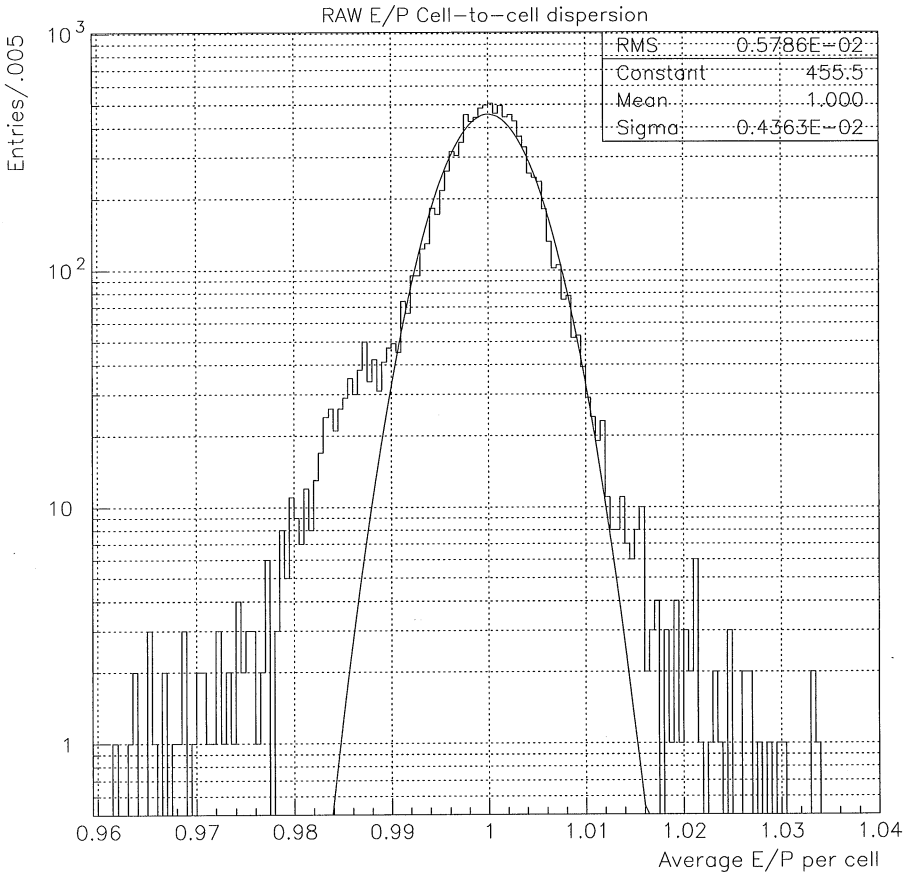

Fig. 9. Cell-to-cell uniformity of the calorimeter, calibrated only electronically.

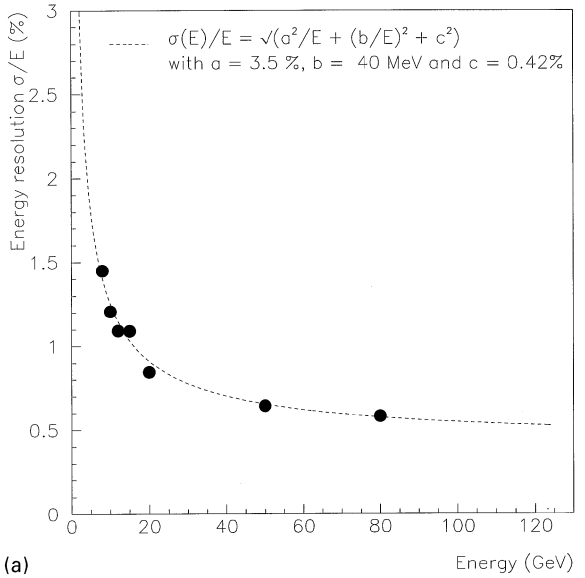

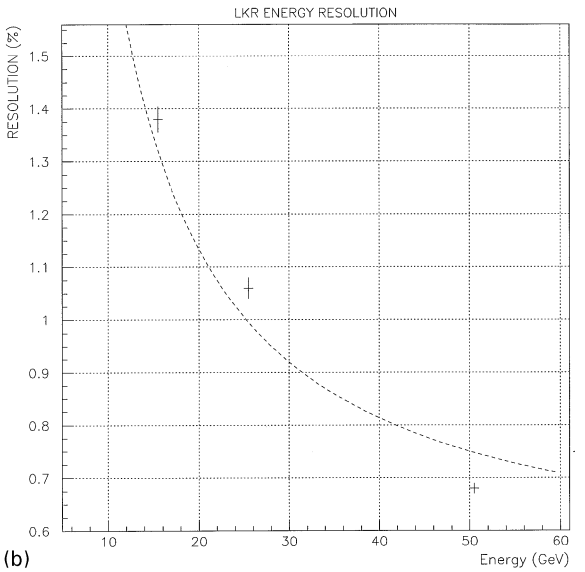

Fig. 10. Energy resolution of the prototype (a) and the 24 ton (b) liquid krypton calorimeter.

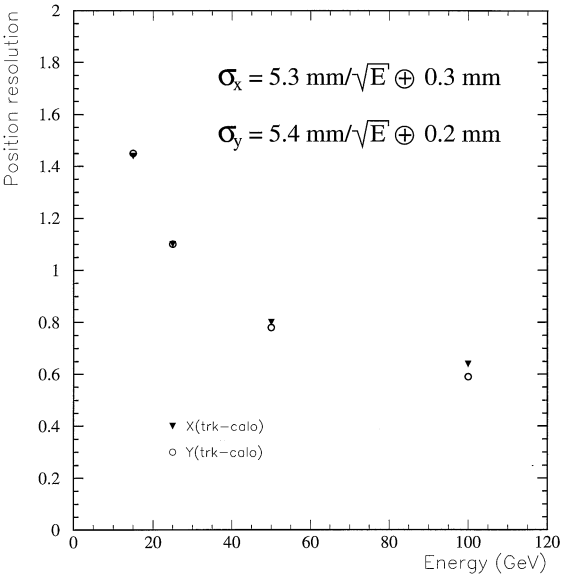

Fig. 11. Position resolution of the NA48 liquid krypton calorimeter.

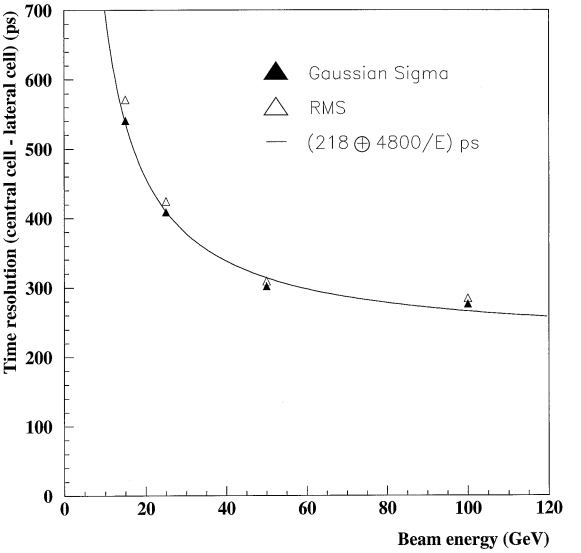

Fig. 12. Time resolution of the calorimeter.

irradiated with electrons from K_{e3} decays. A logarithmic scale was chosen to emphazise the number of cells, deviating from $E/p = 1$. The momentum p of the electrons is measured in the charged particle spectrometer of NA48, the energy of the electron is measured in the liquid krypton calorimeter. Previous to irradiation, the cells had only been calibrated using the electronics calibration system, mentioned above. The uniformity of response is reflected in the small error of 0.4%. Fig. 10a shows the energy resolution of the the prototype calorimeter [16] consisting of 184 cells, and Fig. 10b of the 24 ton liquid krypton calorimeter consisting of

13 248 cells. The dotted line in Fig. 10a is a fit to data point yielding the values for the noise term a, the stochastic term b and the constant term c. The dotted curve in Fig. 10b is the same as in Fig. 10a, except for a higher noise term (from 42 to 130 MeV) and a slightly increased constant term (from 0.42% to 0.5%). The signal-to-noise ratio of both calorimeters differs by a factor of 3, which is due to the fact that the large calorimeter could only be operated 1.5 kV/cm, whereas the prototype calorimeter was operated at 5 kV/cm.[2] Fig. 11 shows the position resolution. The position resolution of an electro-magnetic shower counter depends only on the number of particles in the shower, which is reflected in the $1/\sqrt{E}$ dependence. The tower size of the liquid krypton calorimeter is $\sim \frac{1}{2}R_M$. The time resolution is plotted in Fig. 12. The resolution obtained is $(4.8/E \oplus 0.22)$ ns. Energy, position and time resolution meet the experimental requirements of the CP violation experiment NA48 at CERN.

5. Conclusion

Noble liquid calorimetry either in the form of quasi-homogeneous electromagnetic calorimeters or in the form of sampling calorimeters meets well the requirements of modern high-luminosity experiments. Due to novel concepts, as for example, initial current read-out and longitudinal electrode structures, fast calorimeters with high grain tower geometry can be constructed. Good energy, very good spatial and excellent time resolution have been obtained. Direct calibration and uniformity are the assets of these detectors.

Acknowledgements

I thank my colleagues Alain Givernaud, Augusto Ceccucci and Sandro Palestini for many helpful discussions, which we had during the write-up of this talk. I am grateful to Allain Gonidec and Gunther Fischer for editing this paper, for many suggestions and carefully reading draft after draft. I also wish to express my gratitude to the organizers of the Vienna Conference for their hospitality and for the excellent organization of this conference.

[2] During the winter shut-down of the SPS, the HV problem of the calorimeter was cured and the calorimeter is working at its design voltage since April 1998.

References

[1] U. Amaldi, Physica Scripta 23 (1981) 409.
[2] C.W. Fabjan, T. Ludlam, Ann. Rev. Nucl. Part. Sci. 32 (1982) 335.
[3] C.W. Fabjan, Calorimetry in High Energy Physics, CERN-EP/85-54 Lectures given at the NATO Advanced Studies Institute on Technique and Concepts in High Energy Physics (II). St. Croix,Virgin Islands, USA, 2–13 August 1984.
[4] S. Iwata, Department of Physics Nagoya University, DPNU-13-80. 1980.
[5] T. Virdee, in: A. Eriditato (Ed.), Proc. 2nd Int. Conf. on Calorimetry in High Energy Physics, World Scientific, Singapore.
[6] K. Kleinknecht, in: Th. Ferbel (Ed.), Experimental Techniques in High Energy Nuclear and Particle Physics, World Scientific, Singapore.
[7] Priscilla B. Cushman, in: F. Sauli (Ed.), Instrumentation in High Energy Physics, World Scientific, Singapore.
[8] U. Fano, Phys. Rev. 72 (1) (1947) 26.
[9] ICARUS Proposal, P. Cennini et al., ICARUS II A Second Generation Proton Decay Experiment and Neutrino Observatory at the Gran Sasso Laboratory Vols. I&II, LNGS-94/99-I & LNGS-94/99-II.
[10] Addendum to the ICARUS Proposal, P. Cennini et al., A First 600 Ton ICARUS Detector Installed at the Gran Sasso Laboratory, LNGS-95/10, May 1995.
[11] B. Rossi, High Energy Particles, Prentice-Hall, NY, 1952.
[12] C. Cerri et al., Nucl. Instr. and Meth. 214 (1983) 217.
[13] C. Cerri et al., Nucl. Instr. and Meth. 227 (1984) 227.
[14] V.M. Aulchenko et al., Nucl. Instr. and Meth. A 379 (1996) 475.
[15] D. Fournier, Nucl. Instr. and Meth. A 367 (1995) 5.
[16] G.D. Barr et al., Nucl. Instr. and Meth. A 370 (1996) 413.
[17] W.J. Willis, V. Radeka, Nucl. Instr. and Meth. 120 (1974) 21.
[18] V. Radeka IEEE trans. on Nucl. Sci. NS-24 (1) (1977).
[19] RD3 Proposal, CERN/DRDC/90-31, CERN/DRDC/91-21, and CERN/DRDC/92-40.
[20] ATLAS, Liquid argon calorimeter, Technical Design Report, CERN/LHCC/96-41, 15 December 1996.
[21] ATLAS, Calorimeter performance, CERN/LHCC/96-40, 15 December 1996.
[22] S. Palestini, An electromagnetic calorimeter based on liquid krypton with tower read-out structure, Paper presented at the 1966 IEEE Nuclear Science Symp., 3–9 November 1996, Anaheim, CA.

[23] C. Cerri, Proc. 6th Int. Conf. on Calorimetry in HEP, INFN-LNF, Frascati, 8-14/6/1996.
[24] B. Hallgren et al., IEEE Trans. Nucl. Sci. NS- 43 (3) (1609) 1605.
[25] C. de la Taille et al., NA48 Note 97-30, 18 Dec. 1997.
[26] R. Fantecchi, Paper presented at 2nd Workshop on Electronics for LHC Experiments, Balatonfured, Hungary, 23–17 Sept. 1996.
[27] NA48 Collaboration, Performance and Operation of the 24-ton Liquid Krypton calorimeter for the CP Violation experiment NA48, to be published.